[Article] www.whxb.pku.edu.cn

# 氧化共沉淀法制备 $Ce_{0.65}Zr_{0.25}Y_{0.1}O_{1.95}$ 的结构转化过程

张 磊 郑灵敏 郭家秀 吴冬冬 龚茂初 王健礼 陈耀强*
(四川大学化学学院, 成都 610064)

**摘要:** 以氨水和碳酸铵为沉淀剂, 采用氧化-共沉淀法制备了 $Ce_{0.65}Zr_{0.25}Y_{0.1}O_{1.95}$ 复合氧化物, 并对不同处理温度下制备的样品用热重-差示扫描分析(TG-DSC)、傅里叶变换红外(FT-IR)光谱、X 射线衍射(XRD)和表面分析仪(BET) 等进行了表征. 结果表明, 共沉淀法得到的沉淀物同时含有羟基和羧基, 随着焙烧温度的升高, 分别在 100–170 ℃、250–300 ℃和 420–500 ℃温度范围内先后发生脱水、脱羟基和脱羧基反应, 在此过程中固溶体逐渐形成. 提出了由沉淀物转变为 $Ce_{0.65}Zr_{0.25}Y_{0.1}O_{1.95}$ 复合氧化物的结构转变模型.

**关键词:** $CeO_2$-$ZrO_2$-$Y_2O_3$; 结构转变; 氧化-共沉淀法
**中图分类号:** O643

# Structure Evolution Process of $Ce_{0.65}Zr_{0.25}Y_{0.1}O_{1.95}$ Prepared by Oxidation-Coprecipitation Method

ZHANG Lei ZHENG Ling-Min GUO Jia-Xiu WU Dong-Dong
GONG Mao-Chu WANG Jian-Li CHEN Yao-Qiang*
(*College of Chemistry, Sichuan University, Chengdu 610064, P. R. China*)

**Abstract:** $Ce_{0.65}Zr_{0.25}Y_{0.1}O_{1.95}$ oxides were prepared by oxidation-coprecipitation method using ammonia and salvolatile as precipitators. The as-prepared samples were thermally treated at different temperatures and characterized by thermogravimetry-differential scanning calorimetry (TG-DSC), Fourier transform-infrared (FT-IR) spectrometry, X-ray diffraction (XRD), and specific surface area measurements (BET). The results showed that the hydroxyl and carboxyl groups coexisted in the precipitate and a perfect solid solution was gradually formed with an increase in calcination temperature. The physisorbed water was lost from 100 to 170 ℃, hydroxyl groups were removed from 250 to 300 ℃, and the carboxyl groups were eliminated from 420 to 500 ℃. A structure model was further proposed to understand the $Ce_{0.65}Zr_{0.25}Y_{0.1}O_{1.95}$ structure evolution process in depth.

**Key Words:** $CeO_2$-$ZrO_2$-$Y_2O_3$; Structure evolution; Oxidation-coprecipitation

$CeO_2$ has been widely used in purifying vehicle exhausts and has become the most important rare-earth oxide for controlling $NO_x$. However, the sintering of $CeO_2$ support takes place after calcination at 750 ℃[1]. In recent years, a great interest has been focused on Ce-Zr-O mixed oxides because of their commercial application as automotive three-way catalysts (TWCs)[2–4]. It is reported[5,6] that incorporation of trivalent dopants (such as $Y^{3+}$ and/or $La^{3+}$) into the lattice of the Ce-Zr-O system forms a three-component oxygen storage material (OSM), which possesses a higher catalytic performance. In particular, $CeO_2$-$ZrO_2$-$Y_2O_3$ solid solutions, with a cubic fluorite phase, can improve the thermal stability, specific surface area, and reductive properties of the TWCs. The phase homogeneity of this $CeO_2$-$ZrO_2$-$Y_2O_3$ system relies on its preparation process. The better homogeneity of $CeO_2$-$ZrO_2$-$Y_2O_3$ leads to a higher texture. Therefore, the preparation of homogeneous $CeO_2$-$ZrO_2$-$Y_2O_3$ has been extensively investigated and many researchers have reported the effects of preparation methods on the textural, structural, and redox properties of

Received: January 23, 2008; Revised: April 21, 2008; Published on Web: June 5, 2008.
English edition available online at www.sciencedirect.com
*Corresponding author. Email: yqchen@email.scu.edu.cn; Tel/Fax: +8628-85418451.
国家自然科学基金重点项目(20333030)和国家自然科学基金项目(20773090)资助
© Editorial office of Acta Physico-Chimica Sinica

$CeO_2$-$ZrO_2$-$Y_2O_3$ oxides, such as solid-state synthesis method [7], combustion synthesis method [8], spray pyrolysis method [9], sol-gel [10], and coprecipitation [11]. In these preparation methods, co-precipitation has received considerable attention on account of its simple experimental approach and large-scale production [12–14]. However, any operation step in the preparation procedure has the possibility of phase segregation and inhomogeneous materials.

To solve this issue, a single phase Ce-Zr-O solid solution, only under the condition of a narrow window of preparation, is obtained by adding an ammonium bicarbonate ($NH_4HCO_3$) precipitator into a mixed solution of $Ce(NO_3)_3$ and $Zr(NO_3)_4$ [15]. Homogeneous $CeO_2$-$ZrO_2$ material was prepared by Hori *et al*. [16]. They employed $NH_3\cdot H_2O$ as the precipitating agent and $ZrO(NO_3)_2$ and $(NH_4)_2Ce(NO_3)_6$ as cerium and zirconium precursors, but obtained homogeneous materials with lower surface area (<90 $m^2\cdot g^{-1}$, 500 ℃, 1 h; < 15 $m^2\cdot g^{-1}$, 1000 ℃, 4 h).

In our previous work [17], because the solubility product of $Zr(OH)_4$ ($2\times10^{-48}$) was less than that of $Ce(OH)_3$ ($1.5\times10^{-20}$), although close to $Ce(OH)_4$ ($4\times10^{-51}$), hydrogen peroxide ($H_2O_2$) was used as an oxidative agent to oxidize $Ce^{3+}$ to $Ce^{4+}$. To combine all ions in one compound at a molecular level, Zhao *et al*. [17] used $NH_3\cdot H_2O$ and $(NH_4)_2CO_3$ as bifunctional precipitating agents. The hydroxides were colloidal precipitates, whereas, carbonates were nongelatinous precipitates, but after aging they could obtain a thermodynamic equilibrium and form crystal precipitates. After thermal treatment, the obtained samples showed better thermal stability and weaker agglomeration. This evolution process was comprised of precipitation, dryness, and calcination steps, which had a great effect on the structural and textural properties of materials. However, little attention was focused on the structure of the precipitate evolution to oxides during the different thermal treatment processes. In this study, the structure composition evolution of $CeO_2$-$ZrO_2$-$Y_2O_3$ prepared by oxidation-coprecipitation was investigated.

## 1 Experimental

### 1.1 Preparation of sample

$Ce_{0.65}Zr_{0.25}Y_{0.1}O_{1.95}$ solid solution was prepared by coprecipitation from the corresponding chemicals (AR): $Ce(NO_3)_3\cdot 6H_2O$, $ZrO(NO_3)_2\cdot xH_2O$, and $Y(NO_3)_3\cdot 5H_2O$ at a nominal composition. The precursors were mixed in an aqueous solution, respectively, and an appropriate amount of fresh $H_2O_2$ (30%, *w*) was added to this mixed salt solution. The mixed salt solution was added dropwise to a new container with a mixed solution of ammonia and ammonia-carbonate aqueous solution, to reach a pH value of 10. The precipitate was then aged at the same pH value under vigorous stirring, filtered, and washed with deionized water. Finally, the precipitate was dried at 100 ℃ and calcined at different temperatures (100, 300, 500, and 600 ℃) for 5 h in air, in a muffle furnace. These samples were written as OSM1, OSM2, OSM3, and OSM4, respectively.

### 1.2 Characterization of sample

The BET surface area and pore size distribution of $Ce_{0.65}Zr_{0.25}Y_{0.1}O_{1.95}$ were measured by nitrogen adsorption at liquid $N_2$ temperature (−196 ℃) using a ZXF-6 instrument of surface area (Xibei Chemical Institute, China). To desorb surface impurities, the samples were degassed for 1 h at 300 ℃ in vacuum before commencement of the measurement.

TG and DSC analyses were carried out on a Shimadzu thermal system (Japan) equipped with a working station, typically a 10−15 mg portion of testing materials. The sample was dried at 80 ℃ for 10 h under ambient conditions prior to the TG measurement. The sample was heated from room temperature to 600 ℃ at a rate of 10 ℃·$min^{-1}$ in air atmosphere.

The FT-IR spectra were taken from KBr-supported test materials (<1%, *w*) over the frequency range of 4000–400 $cm^{-1}$ and at 4 $cm^{-1}$ resolution, using a model 2000 Perkin-Elmer FT spectrometer (U.K.). An online data station was used to obtain and handle spectra.

The crystal structures of the samples were determined by X-ray diffraction (XRD) on a DX-1000 diffractometer using Cu $K_\alpha$ radiation ($\lambda$=0.15406 nm) and operating at 40 kV and 25 mA. The XRD data were recorded for 2$\theta$ values between 10° and 90° with a step of 0.02°. The crystalline phases were compared with the reference data from the International Center for Diffraction Data (1999-JCPDS).

## 2 Results and discussion

### 2.1 Role of $H_2O_2$

The influence of $H_2O_2$ on nanocrystalline $CeO_2$ has been investigated by many research groups [18–23]. Djuricic *et al*. [18] have established that the role of $H_2O_2$ is to make it much easier to change the valence state of the cerium ion from Ce(III) to Ce(IV). Scholes *et al*. [19] have also reported that the $O_2^{2-}$ is coordinated to Ce(IV) in a side-on bonding geometry, which appears to hinder the formation of a more extended crystalline $CeO_2$ network. Further investigation [20–23] has also shown that the addition of $H_2O_2$ during the preparation process of $ZrO_2$, $ZrO_2$-$TiO_2$ mixed oxides, $CeO_2$-$La_2O_3$ mixed oxides, and $Y_2O_3$ affects the crystallization behavior of the as-prepared materials. A reaction mechanism between $Zr^{4+}$ and $H_2O_2$ has been proposed [20]:

$$[Zr_4(OH)_8]^{8+}+H_2O_2\rightarrow[Zr_4(OO)_2(OH)_4]^{8+}+4H_2O \quad (1)$$

$$[Zr_4(OO)_2(OH)_4]^{8+}+OH^-\rightarrow Zr(OH)_{4-x}(OOH)_x \quad (2)$$

In the experiment conditions in this study, it was found that when $H_2O_2$ aqueous solution was added to the solution containing $Y^{3+}$ and $Ce^{3+}$ ions, the color of the solution did not change, indicating that $Ce^{3+}$ was not oxidized to $Ce^{4+}$; when $Zr^{4+}$ was introduced to the solution containing $Y^{3+}$ and $Ce^{3+}$ ions, the white solution turned to orange, indicating that the $Ce^{3+}$ ions changed to $Ce^{4+}$ ions. This indicated that $Y^{3+}$ ions could not substitute the role of $Zr^{4+}$ ions.

This $Ce^{4+}$ orange color corresponds to the electronic transition between the center $Ce^{4+}$ ions and the chelating ligand, and not to the electronic 4*f*–4*f* transitions. According to the above-mentioned characteristics, it is proposed that a complex forms be-

tween $H_2O_2$, $Ce^{4+}$ ion, and $Zr^{4+}$ ion. It can be represented in the following form:

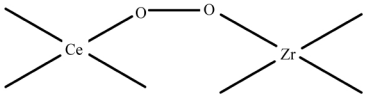


This formation may be attributed to a precipitate, which can form a solid solution after thermal treatment.

### 2.2 Evolution of structure

The BET surface area and total pore volume are listed in Table 1. It can be seen that the surface area decreases, whereas, the pore volume increases with increasing temperature, indicating that the thermal treatment temperature can significantly influence the surface area and pore volume of the sample. The decrease of surface area is the largest from 100 to 300 ℃. The surface area and total pore volume of the sample calcined at 500 ℃ are 120 $m^2 \cdot g^{-1}$ and 0.29 $cm^3 \cdot g^{-1}$. When the calcination temperature is increased to 600 ℃, the surface area and total pore volume of the sample are 118 $m^2 \cdot g^{-1}$ and 0.30 $cm^3 \cdot g^{-1}$. This indicates that the samples calcined at 500 and 600 ℃ exhibit similar textural properties, which may be due to the formation of a stable solid solution.

The TG-DSC patterns of the as-prepared $Ce_{0.65}Zr_{0.25}Y_{0.1}O_{1.95}$ are illustrated in Fig.1. According to the TG-DSC data, the sample is characterized by a 17% total mass loss *via* a rapid mass-loss step ($T$=20–170 ℃), followed by two slow mass-loss steps. The former is an intensely exothermic ($T$=250–300 ℃) process and the latter is a weak endothermic ($T$=420–500 ℃) process. When the temperature is increased from 500 to 600 ℃, no thermal events take place, indicating that a stable solid solution is formed.

It is well-known that the precipitant mainly contains $OH^-$ and $CO_3^{2-}$, and they are incorporated into the network of the precipitate. On the basis of the BET results, it is found that the maximal loss of precipitate takes place at a temperature range of 100–300 ℃. According to a previous investigation[17], the oxygen storage material begins to possess the oxygen storage capacity at 300 ℃ (100 $\mu mol \cdot g^{-1}$) and arrives at a maximum value at 600 ℃ (510 $\mu mol \cdot g^{-1}$). From the TG data, it is confirmed that the as-prepared sample gradually has the structure of an oxygen storage material with the mass loss. This is in agreement with the oxygen storage capacity (OSC) results.

Therefore, it is suggested that the thermal behavior of the sample takes place as follows: first, the endothermic mass-loss step is attributed to the removal of the nondissociative water adsorbed on the surface by the hydrogen bond; second, the exothermic mass-loss step is most probably because of the loss

**Table 1 Influence of calcination temperature on textures of the as-prepared materials**

| Sample | $T$/℃ | $S_{BET}$/($m^2 \cdot g^{-1}$) | $V_{pore}$/($cm^3 \cdot g^{-1}$) |
|---|---|---|---|
| OSM1 | 100 | 218 | 0.20 |
| OSM2 | 300 | 146 | 0.24 |
| OSM3 | 500 | 120 | 0.29 |
| OSM4 | 600 | 118 | 0.30 |

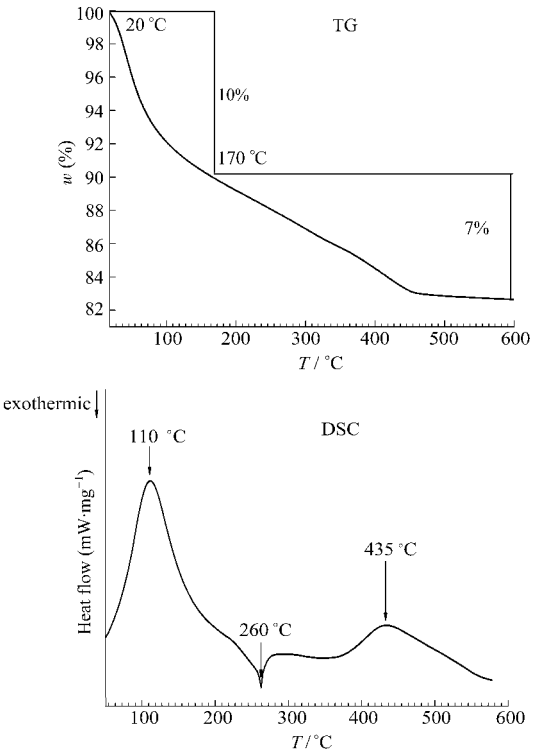


**Fig.1 Thermoanalytical curves for $Ce_{0.65}Zr_{0.25}Y_{0.1}O_{1.95}$**

of water in the micropores and hydroxyl groups; and finally, the endothermic mass-loss process at high-temperature may be considered as a slow decomposition process of the carbonate. A stable solid solution is formed after three mass loss processes.

FT-IR spectra as a function of the calcination temperature of $Ce_{0.65}Zr_{0.25}Y_{0.1}O_{1.95}$ is illustrated in Fig.2. The major features in the IR spectra are in 1350–1700 and 3000–3800 $cm^{-1}$ regions. In addition, the band below 770 $cm^{-1}$ is probably because of the stretching vibration of M—O (M=Ce, Zr). This is observed in the case of $CeO_2$[24]. On the basis of the spectra data, residual water and hydroxyl groups are detected with a large band around 3400 $cm^{-1}$, corresponding to the stretching vibration of the hydroxyl groups. After calcination, the vibration intensity decreases, which is in agreement with the exothermic mass-loss step in the TG curve.

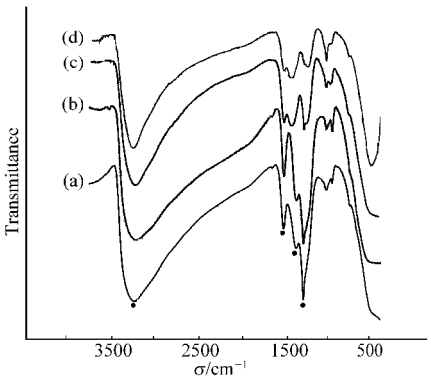


**Fig.2 FT-IR spectra of the as-prepared sample calcined at different temperatures for 5 h**

(a) 100 ℃, (b) 300 ℃, (c) 500 ℃, (d) 600 ℃

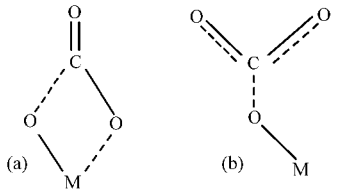


**Fig.3 Schematic representation of (a) bidentate carbonate and (b) unidentate carbonate species**

Another series of strong bands are located at about 1380, 1460, and 1620 $cm^{-1}$, and when the sample is thermally treated at 300 ℃, the intensities of these bands are stronger, but after thermal treatment at 500 ℃, these bands become weaker. This is indicative that they are probably associated with the carbonate species on the oxide surface[25,26], which may be derived from the $(NH_4)_2CO_3$ aqueous solution. It is worth noting that the intensity difference between samples calcined at 500 ℃ for 5 h and at 600 ℃ for 5 h is very small. This indicates that the structure of the as-prepared material changes a little. This is also in agreement with the BET outcome. The broad envelope of bands around 1350−1700 $cm^{-1}$ (Fig.2(a, b)) indicates the presence of different carbonate species. According to the literature data[27], carbonate mainly exists in bidentate (Fig.3(a)) and unidentate carbonate species (Fig.3(b)). Furthermore, unidentate carbonates are more stable than bidentate carbonates.

From the FT-IR experiment, it is confirmed that there are decompositions of carbonates, which could be attributed to the slow endothermic peak around 420−500 ℃ in the TG-DSC test. This is in agreement with the thermal stability of carbonates. On the other hand, it is possible that the bidentate carbonates are first converted into unidentates, and then the unidentate species are removed.

The X-ray diffraction patterns of the synthesized samples are shown in Fig.4. It is found that the powders begin to crystallize at a lower temperature of about 100 ℃. After thermal treatment at 300 ℃, the sample has already displayed the characteristic reflections, which correspond to the fluorite structure of $CeO_2$ (JCPDS: 34-0394). With increasing temperatures, the peak shapes and intensities increase, indicating that the sample can form a perfect crystalline. From the XRD data, no other crystalline phases are detected at any calcination temperature above 300 ℃, indicating that a high homogeneity of solid solution is formed under these experimental conditions. In addition, the diffraction peak intensity of samples calcined at 500 and 600 ℃ are very similar. This is associated with a similar texture of sample calcined at 500 and 600 ℃. Combining with TG results, it is found that the crystalline structure almost does not change when the mass loss of samples occurs, showing that the crystalline growth is only a process of mass transportation.

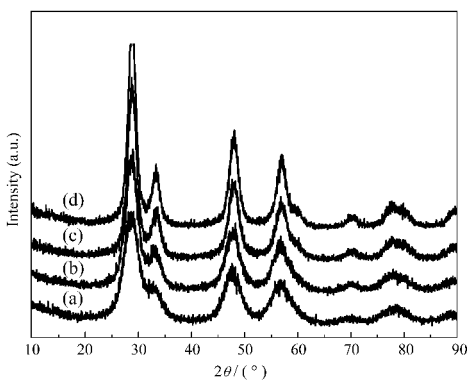


**Fig.4 X-ray diffraction patterns of the as-prepared sample calcined at different temperatures for 5 h**

(a) 100 ℃, (b) 300 ℃, (c) 500 ℃, (d) 600 ℃

### 2.3 Evolution process

To understand the evolution process of a solid solution, a possible schematic route is illustrated in Fig.5. It is found that a solid solution formation is not a simple process. In the precipitate forming process the precipitate possesses a certain extent of crystalline. This consists of $OH^-$, $CO_3^{2-}$, and a water molecule. After drying at 100 ℃, it begins to lose the adhesive moisture. This process mainly takes place at 100−170 ℃. The dehydroxylation step mainly occurs at 250−300 ℃, indicating that the crystallization of the sample is enhanced. With increasing temperature, the precursor is further decomposed into oxides when the calcination temperature is increased to 500 ℃, which is because of oxycarbonate intermediate decomposition. On the other hand, the precursor is decomposed into a solid solution by a transformation from bidentate carbonate to unidentate carbonate intermediate.

From the results of TG-DSC, it is clearly found that there are

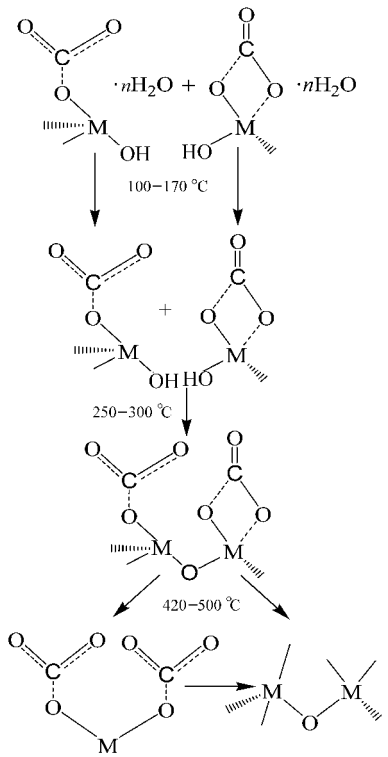


**Fig.5 Schematic representation of structure evolution of the as-prepared oxide (M=Ce or Zr)**

three thermal events at 100–170 ℃, 250–300 ℃, and 420–500 ℃. From the FT-IR spectra, it is seen that the sample treated at 100 ℃ exhibits the typical features of a hydroxyl and carbonate species, indicating that hydroxyl and carbonate species coexist in the initial precipitate. When the treatment temperature is increased to 300 ℃, the band intensity of the hydroxyl groups decreases, whereas, the carboxyl band has no visible change, indicating that the hydroxyl groups are lost from 100 to 300 ℃. When the temperature reaches 500 ℃, the intensity of the carbonate species peaks significantly decreases, and there are no significant differences between the samples treated at 500 and 600 ℃, suggesting that a solid solution is formed. All these characters confirm that the schematic route is reasonable. Combining with the results of BET, OSC, and XRD, it is found that the loss of hydroxyl groups significantly influence the texture, OSC, and crystallization of the samples, although the decarboxyl process has less influence. All the results indicate that many complicated steps occur in the transformation from a precipitate to a stable oxide. Therefore, a homogeneous solid solution can be obtained by gentle and art preparation process.

## 3 Conclusions

With increasing the temperature, the loss of water, dehydroxylation, and removal of carbon dioxide took place in the heat treatment of $Ce_{0.65}Zr_{0.25}Y_{0.1}O_{1.95}$ precipitate. It is worth noting that this structure evolution process is very complicated. From this investigation, it can be seen that the formation of a stable oxide undergoes precipitate forming→dehydration→dehydroxylation→decarboxylation→oxide process. Moreover, $H_2O_2$ plays some important roles in the formation of precipitate homogeneity. For example, $H_2O_2$ has been utilized as an oxidizer to oxidize $Ce^{3+}$ ions to $Ce^{4+}$ ions. However, detailed roles on $H_2O_2$ will be further investigated.

## References


1 Terribile, D.; Trovarelli, A.; Llorca, J.; de Leiten burg, C.; Dolcetti, G. *J. Catal.*, **1998, 178**: 299

2 Trovarelli, A. *Catal. Rev.-Sci. Eng.*, **1996, 38**: 439

3 Kaspar, J.; Fornasiero, P.; Hickey, N. *Catal. Today*, **2003, 77**: 419

4 Gandhi, H. S.; Graham, G. W.; McCabe, R. W. *J. Catal.*, **2003, 216**: 433

5 Kulyova, S. P.; Lunina, E. V.; Lunin, V. V.; Kostyuk, B. G.; Muravyova, G. P.; Kharlanov, A. N. *Chem. Mater.*, **2001, 13**: 1491

6 Ikryannikova, L. N.; Aksenov, A. A.; Markaryan, G. L.; Muraveva, G. P.; Kostyuk, B. G.; Kharlanov, A. N.; Lunina, E. V. *Appl. Catal. A*, **2001, 210**: 225

7 Eguchi, K.; Akasaka, N.; Mitsuyasu, H.; Nonaka, Y. *Solid State Ionics*, **2000, 135**: 589

8 Quinelato, A. L.; Longo, E.; Leite, E. R.; Bernardi, M. I. B.; Varela, J. A. *J. Mater. Sci.*, **2001, 36**: 3825

9 Djurado, E.; Meunier, E. *J. Solid State Chem.*, **1998, 141**: 191

10 Thammachart, M.; Meeyoo, V.; Risksomboon, T.; Osuwan, S. *Catal. Today*, **2001, 68**: 53

11 Hirano, M.; Miwa, T.; Inagaki, M. *J. Ceram. Soc. Jpn.*, **2001, 109**: 401

12 Kirichenko, O. A.; Graham, G. W.; Chun, W.; McCabe, R. W. *Stud. Surf. Sci. Catal.*, **1998, 118**: 411

13 Bozo, C.; Gaillard, F.; Guilhaume, N. *Appl. Catal. A*, **2001, 220**: 69

14 Turko, G. A.; Ivanova, A. S.; Plyasova, L. M.; Litvak, G. S.; Rogov, V. A. *Kinet. Catal.*, **2005, 46**: 884

15 Liu, Y.; Zhai, Y. Q.; Li, Y. D. *React. Kinet. Catal. Lett.*, **2004, 82**: 295

16 Hori, C. E.; Permana, H.; Ng, K. Y.; Brenner, A.; More, K.; Rahmoeller, K. M.; Belton, D. *Appl. Catal. B*, **1998, 16**: 105

17 Zhao, M.; Guo, J. X.; Liu, P.; Fang, H.; Cai, L.; Mao, X. B.; Gong, M. C.; Chen, Y. Q. *Chin. J. Inorg. Chem.*, **2006, 22**(6): 1123 [赵 明, 郭家秀, 刘 萍, 房 华, 蔡 黎, 毛小波, 龚茂初, 陈耀强. 无机化学学报, **2006, 22**(6): 1123]

18 Djuricic, B.; Pickering, S. *J. Eur. Ceram. Soc.*, **1999**, **19**: 1925

19 Scholes, F. H.; Hughes, A. E.; Hardin, S. G.; Lynch, P.; Miller, P. R. *Chem. Mater.*, **2007**, **19**: 2321

20 Cho, S. K.; Kim, I. T.; Kim, D. Y.; Kim, B. K.; Lee, J. H.; Park, S. J. *Mater. Lett.*, **1997, 32**: 271

21 Navio, J. A.; Colon, G.; Sanchez-Soto, P. J.; Macias, M. *Chem. Mater.*, **1997, 9**: 1256

22 Colon, G.; Navio, J. A.; Monaci, R.; Ferino, I. *Phys. Chem. Chem. Phys.*, **2000, 2**: 4453

23 Henryk, T.; Helena, W.; Roger, D. G. *J. Eur. Ceram. Soc.*, **1997, 17**: 403

24 Tommy, M.; Ingeborg, K.; Tor, G.; Mari-Ann, E. *Chem. Mater.*, **2004, 16**: 5489

25 Li, C.; Sakata, Y.; Arai, T.; Domen, K.; Maruya, K. I.; Onishi, T. *J. Chem. Soc., Faraday Trans.*, **1989, 85**: 929

26 Li, C.; Sakata, Y.; Arai, T.; Domen, K.; Maruya, K. I.; Onishi, T. *J. Chem. Soc., Faraday Trans.*, **1989, 85**: 1451

27 Bolis, V.; Magnacca, G.; Cerrato, G.; Morterra, C. *Thermochim. Acta*, **2001, 379**: 147